

ARTICLE

## Smoldering combustion in cellulose and hemicellulose mixtures: Examining the roles of density, fuel composition, oxygen concentration, and moisture content

W. Jayani Jayasuriya, Tejas Chandrashekhar Mulky, and Kyle E. Niemeyer

School of Mechanical, Industrial, and Manufacturing Engineering, Oregon State University,  
Corvallis, OR, USA

### ARTICLE HISTORY

Compiled June 9, 2022

### Abstract

Smoldering combustion plays a key role in wildfires in forests, grasslands, and peatlands due to its common occurrence in porous fuels like peat and duff. As a consequence, understanding smoldering behavior in these fuels is crucial. Such fuels are generally composed of cellulose, hemicellulose, and lignin. Here we present an updated computational model for simulating smoldering combustion in cellulose and hemicellulose mixtures. We used this model to examine changes in smoldering propagation speed and peak temperatures with varying fuel composition and density. For a given fuel composition, increases in density decrease the propagation speed and increase mean peak temperature; for a given density, increases in hemicellulose content increase both propagation speed and peak temperature. We also examined the role of natural fuel expansion with the addition of water. Without expansion, addition of moisture content reduces the propagation speed primarily due to increasing (wet) fuel density. However, with fuel expansion similar to that observed in peat, the propagation speed increases due to the overall drop in fuel density. Finally, we studied the influence of fuel composition on critical moisture content of ignition and extinction: mixtures dominated by hemicellulose have 10% higher critical moisture content due to the increase in peak temperature.

### KEYWORDS

wildland fires; smoldering combustion; cellulose; hemicellulose

## 1. Introduction

Wildland fires lead to human, environmental, and ecological hazards. Global climate change has and will continue to cause increases in the occurrence of droughts, which will in turn lead to an increasing frequency of wildland fires [1, 2]. Combustion in wildland fires, in general, is dominated by either flaming or smoldering combustion. Both types of combustion have different characteristics and can be hazardous in their own way, but flaming combustion has historically received more research compared with smoldering. However, as Rein [3] discussed, smoldering combustion has recently become more recognized as a major fire hazard, resulting in increasing interest in understanding this phenomenon.

Compared with flaming combustion, smoldering can persist longer and under conditions that would extinguish flames. This characteristic of smoldering combustion allows it to penetrate deeper into the soil compared with flaming combustion, which generally causes shallower burns [4, 5]. Thus, smoldering can actually cause greater destruction in affected ecosystems. Smoldering also emits a large number of pollutants such as carbon monoxide (CO), volatile organic compounds, polycyclic aromatic hydrocarbons, and particulate matter, since it operates at lower temperatures than flaming combustion. Smoldering occurs most commonly in porous fuels like peat, woody fuels, muck, and forest duff [2]. Such fuels are abundant in forests, making it important to understand smoldering combustion in these types of fuels. Woody fuels and biomass generally consist of cellulose, hemicellulose, and lignin in varying proportions, which pyrolyze at different temperatures as shown by Ranzi et al. [6, 7]. Yang et al. [8] found that, among the three, hemicellulose pyrolyzes earliest, at temperatures of 220–315 °C, cellulose undergoes pyrolysis at temperatures of 315–400 °C, and finally lignin pyrolyzes at temperatures of 150–900 °C. Anca-Couce et al. [9] showed similar trends in pyrolysis of these three constituents in their thermogravimetric analysis of pine wood. In addition, these fuel constituents produce different amounts of char [10–12]. Smoldering combustion is generally modeled using a set of global reactions, which include fuel pyrolysis and char oxidation [9, 13]. Differences in fuel composition thus may lead to significant differences in smoldering characteristics. This motivates our detailed study looking into how varying fuel composition affects smoldering characteristics.

Along with fuel composition, the other parameters that could affect smoldering propagation are density and moisture content. Huang and Rein [14] found that increasing the density of peat by 40% reduces the downward propagation speed by approximately 40%. However, no (computational) studies have looked into how changes in density affect smoldering speed and temperatures in fuel mixtures of cellulose and hemicellulose. In contrast, regarding the effects of moisture content, Huang and Rein [14] studied how moisture content affects the propagation speed of peat and observed an increase in downward propagation speed with moisture content, due to expansion of the peat. Recently, Smucker et al. [15, 16] experimentally observed that smoldering propagation speed in mixtures of cellulose and hemicellulose decreases with density, and attributed this to oxygen availability. They also found that propagation speed increases with additional hemicellulose content in fuel, attributed to faster pyrolysis with addition of hemicellulose, from its lower activation energy and higher heat release.

Critical moisture content is the highest moisture content above which smoldering combustion cannot self-sustain. Garlough and Keyes [17] experimentally studied ponderosa pine duff and found that fuel consumption decreases after reaching critical moisture content of 57 and 102% on the upper and lower duff, respectively. Frandsen showed experimentally that duff’s critical moisture content of ignition drops with inorganic content [18, 19]. Huang and Rein [20, 21] found that natural peat’s critical moisture contents of ignition and extinction are around 117% and 250%, respectively, but vary significantly depending upon the thickness of wet layer, dry layer, inorganic content, physical properties, and boundary conditions. However, no studies have looked into the influence of the fuel composition on these threshold values.

In our prior work, we found that propagation speed increases as density drops or hemicellulose content increases for mixtures of cellulose and hemicellulose [22]. Based on prior theories in the literature, we hypothesized that oxygen availability causes the sensitivity to density, and that adding hemicellulose increases propagation speed since it pyrolyzes faster. However, that study did not include an in-depth analysis to examine the proposed hypotheses or their fundamental causes. In addition, for validating the

model with experimental results, we relied on a fixed temperature boundary condition, which overconstrained the model. Furthermore, our previous treatment of bulk density for validation case may not represent actual experimental conditions: we fixed the bulk density of hemicellulose and changed the bulk density of cellulose to match the mixture bulk density; in experiments, they change together [15, 16, 23]. The model used in that work did not predict ignition for bulk densities of less than 200 kg/m<sup>3</sup> for 100% cellulose, which disagrees with experimental observations [15, 16]. Here, we use a more-appropriate boundary condition at the upper surface, allow the bulk density of the fuel components to vary independently, and updated physical property values (e.g., particle surface area). This study also expands on the analysis of the reasons behind observed trends in propagation speed and peak temperature, confirms the relationship between oxygen availability and density posited for peat by Huang and Rein [14], confirms—and extend to general fuels—the observation by Huang and Rein [14] that moisture content increases downward smoldering in peat, and also examines the impact of fuel composition on critical moisture content of ignition and extinction.

Building on our prior work, this article presents an updated one-dimensional, transient computational model to simulate smoldering combustion in cellulose and hemicellulose mixtures. First, we validate the model against a different experimental configuration that more closely matches the simulation, and use a heat-flux boundary condition. Following this model validation, we examine the effects of varying density and fuel composition on smoldering propagation speed and peak temperature, and perform an in-depth analysis to explain the observed trends. Next, we investigate the effects of varying moisture content on smoldering propagation speed and temperature, including and excluding the contribution of fuel expansion with the addition of water. Finally, we identify how varying fuel composition affects the critical moisture content of ignition and extinction.

## 2. Computational model

In this article, we study downward propagation of smoldering using a one-dimensional transient model following approaches of past studies [22]. This model was developed using Gpyro [24]. We performed simulations with a spatial cell size ( $\Delta z$ ) of  $1 \times 10^{-4}$  m and an initial time step of 0.05 s. We based this selection of cell size on our previous work, where we showed that further increasing resolution has little impact on global quantities of interest [22].

### 2.1. Governing equations

To model smoldering combustion, we use Gpyro v0.700 [24, 25] to solve the transient governing equations: condensed-phase mass conservation (1), condensed-phase species conservation (2), gas-phase mass conservation (3), gas-phase species conservation (4), condensed-phase energy conservation (5), gas-phase momentum conservation (6), and gas-phase energy conservation (7); the ideal gas equation of state (8) is needed to close the set of equations. Lautenberger and Fernandez-Pello [25] provide more details about Gpyro. For completeness, the governing equations are:

$$\frac{\partial \bar{\rho}}{\partial t} = -\dot{\omega}_{fg}''', \quad (1)$$

$$\frac{\partial(\bar{\rho}Y_i)}{\partial t} = \dot{\omega}_{fi}''' - \dot{\omega}_{di}''' , \quad (2)$$

$$\frac{\partial(\rho_g\bar{\psi})}{\partial t} + \frac{\partial\dot{m}''}{\partial z} = \dot{\omega}_{fg}''' , \quad (3)$$

$$\frac{\partial(\rho_g\bar{\psi}Y_j)}{\partial t} + \frac{\partial(\dot{m}''Y_j)}{\partial z} = -\frac{\partial}{\partial z}(\bar{\psi}\rho_g D \frac{\partial Y_j}{\partial z}) + \dot{\omega}_{fj}''' - \dot{\omega}_{dj}''' , \quad (4)$$

$$\begin{aligned} \frac{\partial(\bar{\rho}h)}{\partial t} &= \frac{\partial}{\partial z}(\bar{k} \frac{\partial T}{\partial z}) - \dot{Q}_{s-g}''' + \sum_{k=1}^K \dot{Q}_{s,k}''' - \frac{\partial\dot{q}_r''}{\partial z} \\ &+ \sum_{i=1}^M ((\dot{\omega}_{fi}''' - \dot{\omega}_{di}''')h_i) , \end{aligned} \quad (5)$$

$$\dot{m}'' = -\frac{\bar{K}}{v} \frac{\partial P}{\partial z} , \text{ and} \quad (6)$$

$$\begin{aligned} \frac{\partial(\bar{\psi}\rho_g\bar{h}_g)}{\partial t} + \frac{\partial(\dot{m}_z''\bar{h}_g)}{\partial z} &= \frac{\partial}{\partial z}(\bar{\psi}\rho_g D \frac{\partial\bar{h}_g}{\partial z}) + h_{cv}(T - T_g) \\ &+ \sum_{j=1}^N (\dot{\omega}_{s,fj}''' - \dot{\omega}_{s,dj}''')h_{g,j}^* + \dot{Q}_{s-g}''' , \end{aligned} \quad (7)$$

$$P\bar{M} = \rho_g R T_g , \quad (8)$$

where  $\rho$  is the density,  $M$  is the number of condensed-phase species;  $X$  is the volume fraction;  $\dot{\omega}'''$  is the reaction rate;  $T$  is the temperature;  $Y_j$  is the  $j$ th species mass fraction;  $\psi$  is the porosity;  $K$  is the permeability/number of reactions;  $h_{cv}$  is the volumetric heat transfer coefficient;  $\bar{M}$  is the mean molecular mass obtained from local volume fractions of all gaseous species;  $\dot{q}_r''$  is the radiative heat-flux;  $\dot{Q}'''$  is the volumetric rate of heat release/absorption;  $R$  is the universal gas constant;  $D$  is the diffusion coefficient;  $h$  is the enthalpy;  $P$  is the pressure; subscripts  $f$ ,  $d$ ,  $i$ ,  $j$ ,  $k$ ,  $s$ , and  $g$  are formation, destruction, condensed-phase species index, gas-phase species index, reaction index, solid, and gas; and \* indicates that gas-phase species enthalpy is calculated at condensed phase temperature. The overbars over  $\rho$ ,  $\psi$ ,  $K$ , and  $k$  mean an averaged value weighted by condensed-phase volume fraction, while the overbar over  $h$  indicates an averaged value weighted by condensed-phase mass fraction.

## 2.2. Boundary conditions

The top surface ( $z = 0$ ) of the domain was modeled as open to atmosphere while the bottom surface ( $z = L$ ) was modeled as insulated to match the experimental setup, as Figure 1 shows. The pressure ( $P$ ) at the top surface was 1 atm and the ambient temperature was 300 K. On the top surface we set a convective heat transfer coefficient ( $h_{c,0}$ ) as 10 W/m<sup>2</sup>K using an empirical correlation of  $h_{c,z=0} = 1.52 \times T^{1/3}$  where  $T = 300$  K [21]. At the upper surface we also set the mass-transfer coefficient ( $h_{m,0}$ ) at 0.02 kg/m<sup>2</sup> sec based on previous work [21]. To ignite the sample we provided a heat flux ( $\dot{q}_e''$ ) of 25 kW/m<sup>2</sup> for 20 min at the top boundary to establish self-sustained smoldering, after which we removed the heat flux and established a convective–radiative balance

at the top surface (e.g., for  $t > 20$  min):

$$-\bar{k} \frac{\partial T}{\partial z} \Big|_{z=0} = -h_{c0}(T_{z=0} - T_\infty) + \bar{\epsilon} \dot{q}_e'' - \bar{\epsilon} \sigma (T_{z=0}^4 - T_\infty^4) , \quad (9)$$

$$-\bar{k} \frac{\partial T}{\partial z} \Big|_{z=0} = -h_{c0}(T_{z=0} - T_\infty) - \bar{\epsilon} \sigma (T_{z=0}^4 - T_\infty^4) , \quad (10)$$

$$-\left( \bar{\psi} \rho_g D \frac{\partial Y_j}{\partial z} \right) \Big|_{z=0} = h_{m0} (Y_{j\infty} - Y_j|_{z=0}) , \text{ and} \quad (11)$$

$$P|_{z=0} = P_\infty . \quad (12)$$

We applied these boundary conditions for all simulations, except those looking at the effects of varying moisture content on propagation speed (Sec. 3.3) where we set a constant heat flux throughout the simulation to guarantee ignition at higher moisture contents.

For the bottom surface we set a heat-transfer coefficient ( $h_{c,L}$ ) of 3 W/m<sup>2</sup>K to account for losses through the insulation. The mass flux ( $\dot{m}''$ ) was set to zero at the bottom surface. The equations used for boundary conditions on the bottom surface are

$$-\bar{k} \frac{\partial T}{\partial z} \Big|_{z=L} = -h_{cL}(T|_{z=L} - T_\infty) , \text{ and} \quad (13)$$

$$-\left( \bar{\psi} \rho_g D \frac{\partial Y_j}{\partial z} \right) \Big|_{z=L} = 0 . \quad (14)$$

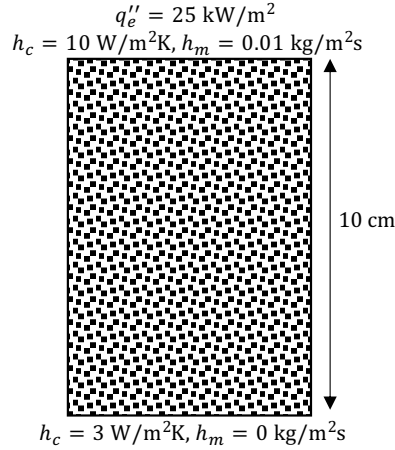
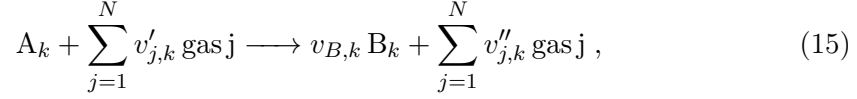


**Figure 1.** Schematic illustration of the one-dimensional computational domain.

### 2.3. Chemical kinetics

Gpyro represents heterogeneous reactions as [25]:



where  $k$  represents the reaction number,  $A_k$  and  $B_k$  are condensed-phase species,  $v'_{j,k}$  and  $v''_{j,k}$  are the reactant and product stoichiometric coefficients for gas  $j$  in reaction  $k$ ,  $v_{B,k}$  is the stoichiometric coefficient for condensed-phase species  $B$  in reaction  $k$ , and  $N$  is the total number of gas-phase species. The reaction rates are expressed in Arrhenius form:

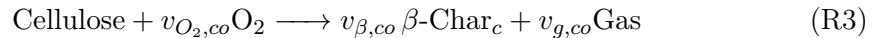
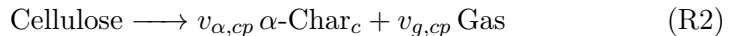
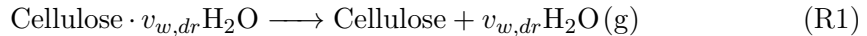
$$\dot{\omega}'_{dA_k} = Z_k \frac{(\bar{\rho} Y_{A_k} \Delta z)_{\Sigma}}{\Delta z} \left( \frac{\bar{\rho} Y_{A_k} \Delta z}{(\bar{\rho} Y_{A_k} \Delta z)_{\Sigma}} \right)^{n_k} \times \exp \left( -\frac{E_k}{RT} \right) g(Y_{O_2}), \quad (16)$$

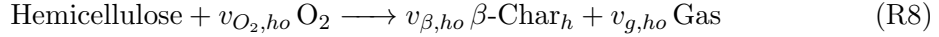
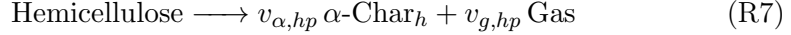
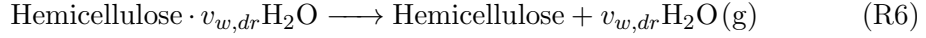
where

$$(\bar{\rho} Y_{A_k} \Delta z)_{\Sigma} = \bar{\rho} Y_{A_k} \Delta z|_{t=0} + \int_0^t \dot{\omega}'_{fi}(\tau) \Delta z(\tau) d\tau, \quad (17)$$

$Z$  is the pre-exponential factor,  $E$  is the activation energy,  $n$  is the order of reaction, subscript  $dA$  stands for destruction of species  $A$ , and subscripts  $k$ ,  $f$ , and  $i$  are reaction index, formation, and condensed-phase species index. In Eq. (16), for inert atmosphere  $g(Y_{O_2}) = 1$  and when oxygen is available  $g(Y_{O_2}) = (1 + Y_{O_2})^{n_{O_2,k}} - 1$  [25].

We represent the smoldering process with a system of global pyrolysis and oxidation reactions [13, 26], using the model developed by Huang and Rein [10, 27] for smoldering of the mixtures of interest. In this model, moist fuel dries, then the dried fuel thermally decomposes to form char by two paths: fuel pyrolysis and fuel oxidation.  $\alpha$ -Char forms via fuel pyrolysis while  $\beta$ -char forms from fuel oxidation. Next,  $\alpha$ - and  $\beta$ -char oxidize and form ash. The drying and fuel-pyrolysis reactions are endothermic reactions while the fuel- and char-oxidation reactions are exothermic. When considering 100% cellulose (i.e., neat cellulose) the model contains five global reactions, while for mixtures of cellulose and hemicellulose the model includes 10 global reactions. The full 10-step chemical kinetic model follows:





where  $v$  is the stoichiometric coefficient;  $\alpha$  and  $\beta$  indicate char produced from fuel pyrolysis and fuel oxidation reactions, respectively; and subscripts  $w$ ,  $g$ ,  $O_2$ ,  $a$ ,  $c$ ,  $h$ ,  $dr$ ,  $o$ ,  $p$ ,  $\alpha o$ ,  $\beta o$  are water, gas, oxygen, ash, cellulose, hemicellulose, drying, oxidation, pyrolysis,  $\alpha$ -char oxidation, and  $\beta$ -char oxidation, respectively.

Table 1 lists the chemical-kinetic parameters (pre-exponential factor, activation energy, order of reaction, and heat of reaction) for the schemes used here, obtained from Huang and Rein [10]. They developed the model to simulate smoldering of biomass, by optimizing kinetic parameters to match thermogravimetric-analysis measurements using a genetic algorithm [28]. We chose the kinetic parameters based on experiments using low-mineral moss peat (2.1% inorganic content), with oxygen concentrations of 0, 10, and 21 % and heating rates of 10, 20, and 30 K/min; the optimized model showed a minimum error of 5.5% with respect to the experimental measurements. Here, we apply this model to simulate smoldering in more-general mixtures of cellulose and hemicellulose. We accounted for the consumption of oxygen using the relation  $v_{O_2,k} = \Delta H / (-13.1) \text{ MJ/kg}$  [21, 29].

**Table 1.** Kinetic parameters for cellulose and hemicellulose model.

Reaction number	Reaction	Cellulose				
		$\log Z$ $\log \text{s}^{-1}$	$E$ kJ/mol	$\Delta H$ MJ/kg	$n$ -	$n_{O_2}$ -
(R1)	Drying	8.12	67.8	2.26	2.37	-
(R2)	Pyrolysis	11.7	156	0.5	1	-
(R3)	Oxidation	24.2	278	-28.2	1.73	0.74
(R4)	$\beta$ -char oxidation	7.64	120	-28.8	1.25	0.89
(R5)	$\alpha$ -char oxidation	12.2	177	-27.8	0.93	0.52
Reaction Number	Reaction	Hemicellulose				
		$\log Z$ $\log \text{s}^{-1}$	$E$ kJ/mol	$\Delta H$ MJ/kg	$n$ -	$n_{O_2}$ -
(R6)	Drying	8.12	67.8	2.26	2.37	-
(R7)	Pyrolysis	6.95	93.8	0.5	0.98	-
(R8)	Oxidation	20.2	294	-20.9	0.47	0.11
(R9)	$\beta$ -char oxidation	7.64	120	-28.8	1.25	0.89
(R10)	$\alpha$ -char oxidation	12.2	177	-27.8	0.93	0.52

#### 2.4. Physical properties

Table 2 reports the physical properties of condensed-phase species: solid density ( $\rho_{s,i}$ ), thermal conductivity ( $k_{s,i}$ ), and heat capacity ( $c_i$ ). For the natural bulk densities of cellulose and hemicellulose ( $\rho_i$ ), we used the values experimentally measured by Cowan et al. [30]: 175 kg/m<sup>3</sup> and 695.71 kg/m<sup>3</sup>, respectively. (Bulk density refers to the density of the species including pores, i.e., total mass divided by total volume, while solid density is the density of the species without any pores.) We calculated the bulk density of char using the correlation  $\rho_{\text{char}} \approx v_{\text{char}} \times \rho_{\text{fuel}}$  [14] and the bulk density of ash using  $\rho_{\text{ash}} \approx \text{AC}/100 \times 10 \times \rho_{\text{fuel}}$ , where AC stands for ash content [31]. The ash contents of cellulose and hemicellulose are 0.3% and 1.2%, respectively [10, 32, 33]. Following the

studies of Huang et al. [21], we assumed the solid physical properties of fuels do not depend on temperature.

**Table 2.** Thermophysical properties of condensed-phase species, taken from the literature for water [10], cellulose [34], hemicellulose [35–37], char [10, 38], and ash [10, 38].

Species	Solid density, $\rho_{s,i}$ (kg/m <sup>3</sup> )	Thermal conductivity, $k_{s,i}$ (W/(m K))	Heat capacity, $c_i$ (J/(kg K))
Water	1000	0.6	4186
Cellulose	1500	0.356	1674
Hemicellulose	1365	0.34	1200
Char	1300	0.26	1260
Ash	2500	1.2	880

The effective thermal conductivity of a condensed-phase species is calculated using

$$k_i = k_{s,i}(1 - \psi_i) + \gamma_i \sigma T^3, \quad (18)$$

where  $k_{s,i}$  is the solid thermal conductivity of species  $i$ ,  $\psi_i$  is the porosity of species  $i$ ,  $\sigma$  is the Stefan–Boltzmann constant, and  $\gamma_i$  is an empirical parameter for radiation across pores that depends on pore size [25]. The porosity of species  $i$  is calculated with

$$\psi_i = 1 - \frac{\rho_i}{\rho_{s,i}}. \quad (19)$$

Pore size,  $\gamma_i$ , and permeability are calculated for each condensed-phase species at their natural densities using

$$d_{po,i} \approx d_{p,i} = \frac{1}{S_i \times \rho} \quad (20)$$

$$K_i = 10^{-3} \times d_{p,i}^2 \quad (21)$$

$$\gamma_i = 3 \times d_{po,i}, \quad (22)$$

where  $\rho$  is the density of the fuel,  $S_i$  is the particle surface area for species  $i$ ,  $d_{p,i}$  is the particle size,  $K_i$  is the permeability, and  $d_{po,i}$  is the pore size [10, 21, 39, 40]. The particle surface areas of cellulose, cellulose-based ash, hemicellulose, and hemicellulose-based ash are 0.0388, 0.1533, 0.0678, and 0.2712 m<sup>2</sup>/g, respectively [10, 41–43]. These correlations apply at the natural densities of the fuels based on the assumption of similar particle and pore size [10, 21]. For cases where we model fuels with specific or varying densities, we assigned this value as the natural density and used Eqs. (20)–(22) to vary properties with density.

However, when we emulate increases in density due to compression, the particle size  $d_{p,i}$  remains constant but pore size  $d_{po,i}$  decreases due to the reduction of pore volume. Thus, when validating our model (Section 3.1), we used the experimental measurements of Smucker et al. [15, 16] for bulk density; they changed the density of fuels by compressing the samples from their natural density to reach the desired density. To model this compression, we account for the associated changes in pore size ( $d_{po,i}$ ) and radiation parameter ( $\gamma_i$ ) by scaling them with change in porosity ( $\psi$ ), since porosity is directly proportional to the volume occupied by pores. Permeability also



changes during compression, which we vary with the Kozeny–Carman equation:

$$K_i \propto \frac{e_i^3}{1 + e_i} , \quad (23)$$

where  $e_i$  is the void ratio, related to porosity with  $e_i = \psi_i/(1 - \psi_i)$ .

Unless mentioned otherwise, we ran all simulations with 10% moisture content to account for moisture content already present in natural fuels and moisture absorbed from the atmosphere [10, 14]. The addition of water changes the density of the (wet) fuel, and we accounted for this change using

$$\rho_{\text{wet fuel}} = \rho_{\text{dry fuel}} \times (1 + \text{MC}) , \quad (24)$$

where MC is the moisture content [21]. To investigate the role of this natural fuel expansion, we considered cases where the fuel expands with moisture content and where it does not; when the fuel does expand, we use the correlation developed for peat by Huang and Rein [14] with the bulk density modified for the fuels considered here. Porosity changes less than 5% with this change in density here, so we consider this adoption justified. The modified correlation is

$$\rho_{\text{dry fuel}} = \frac{200 + 40\text{MC}}{1 + \text{MC}} . \quad (25)$$

Thermal conductivity ( $k$ ) and heat capacity ( $c$ ) also vary with moisture content, and we change those for wet fuels by averaging using volume fraction ( $X_i$ ) and mass fraction ( $Y_i$ ), respectively [21, 25]:

$$k_{\text{wet fuel}} = X_{\text{H}_2\text{O}}k_{\text{H}_2\text{O}} + X_{\text{dry fuel}}k_{\text{dry fuel}} \quad (26)$$

$$c_{\text{wet fuel}} = Y_{\text{H}_2\text{O}}c_{\text{H}_2\text{O}} + Y_{\text{dry fuel}}c_{\text{dry fuel}} . \quad (27)$$

## 2.5. Calculation of global quantities

The two main parameters of interest in this study are mean propagation speed of smoldering and mean peak temperature. We calculate propagation speed by numerically computing the derivative of depth with respect to time of peak temperature; in other words, the difference between two depths divided by the times when those depths reach their maximum temperature. Figure 2 shows an example temperature vs. time profile that demonstrates how we record the data for calculating these global quantities. This requires selecting a depth interval for evaluating this finite difference; to determine the appropriate interval value for calculating mean propagation speed, starting at 6 cm we systematically reduced the depth interval and examined the effect on calculated mean propagation speed. (A smaller depth interval requires both producing and evaluating more data from the simulations, so we seek a pragmatic choice that affects the results little while reducing the computational burden.) After reducing the depth interval to 1 cm, further reduction negligibly affects propagation speed: reducing from 1 cm to 0.5 cm increases the calculated speed by less than 0.3%. As a result, we chose a depth interval of 1 cm for all cases. The supplementary material shows the effects of reducing depth interval on propagation speed in more detail. We calculated mean peak temperature similarly by averaging the peak temperatures every 1 cm.

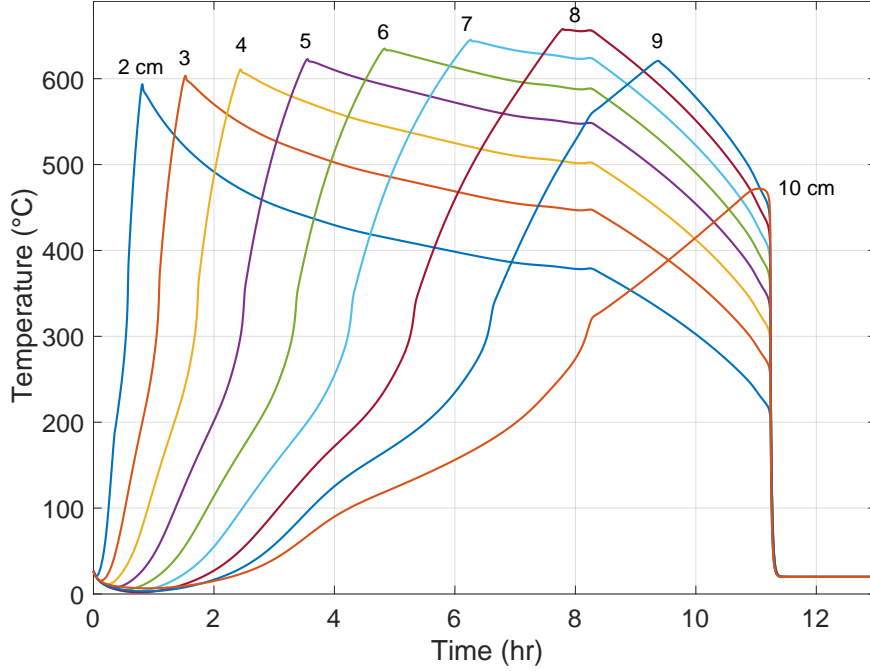


**Figure 2.** Temperature profile with respect to time for a fuel composition of 50% cellulose at a density of  $300 \text{ kg/m}^3$ .

### 3. Results and discussion

First, we validated the model by comparing it with experimental measurements of mean propagation speed and mean peak temperature. Then, we varied density and fuel composition to study how these parameters affect smoldering behavior. Next, we examined the effect of moisture content on mean peak temperature and mean propagation speed for 100% cellulose. Finally, we examined how the critical moisture content of ignition and extinction change with fuel composition.

#### 3.1. Validation

We validated the computational model using the experimental results of Smucker et al. [15, 16] by comparing two parameters: mean peak temperature and mean propagation speed. The experiments used a one-dimensional reactor box of dimensions  $10 \text{ cm} \times 10 \text{ cm} \times 13 \text{ cm}$ , with thermocouples placed at 1 cm depth intervals. The top surface of the reactor box was open to atmosphere and the other sides were insulated using a calcium silicate insulation board, and the fuel samples were ignited using a cartridge heater applied until the point of self-sustained smoldering. The supplemental material contains key information about the experimental measurements, and Smucker et al. [15, 16] provide further details about the experimental configuration.

To ensure self-sustained smoldering, we performed our validation simulations using a heat flux of  $25 \text{ kW/m}^2$  applied for 20 min at the top surface. However, we found that smoldering behavior was insensitive to the magnitude of the heat flux; doubling it changed the propagation speed by less than 1.8%. This gave us the confidence to use heat flux as the boundary condition to ignite the fuel sample.

We used eight fuel samples with varying fuel composition and density to validate the

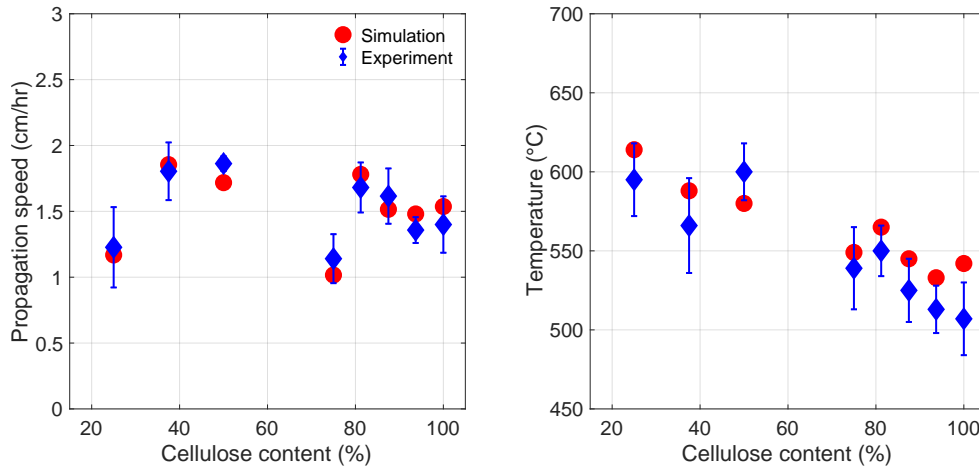


**Figure 3.** Experimental (diamond) and predicted (circle) propagation speeds and mean peak temperatures (filled symbols) for fuel compositions of 25, 50, 75, and 100% cellulose at densities of 400, 250, 300, and 170 kg/m<sup>3</sup>.

model: 25, 37.5, 50, 75, 81.2, 87.5, 93.7, and 100% cellulose, with the remainder hemicellulose, at respective densities of 400, 200, 250, 300, 250, 250, 250, and 170 kg/m<sup>3</sup>. They created these mixtures artificially by mixing the two components and then compressing the fuel to achieve a desired density. Figure 3 compares the experimental measurements and model calculations of mean propagation speed and peak temperature; the model captures all of the experimentally observed trends, and also agrees well quantitatively. The model overpredicts mean propagation speed for 100% cellulose by 10.8% in the worst case, while the average error in propagation speed for the four mixtures is 8.7%. Similarly, the model overpredicts mean peak temperature for 100% cellulose in the worst case by 6.1%, with the average error at 5.3%. Based on these results, we will use this model for the remaining studies here.

### 3.2. Sensitivity to fuel composition and density

Next, we investigated the effects of density and fuel composition on mean peak temperatures, as Figure 4 shows. We artificially created these mixtures to analyze the effects of fuel composition and density on smoldering behavior. We varied fuel density between 200–400 kg/m<sup>3</sup> in increments of 50 kg/m<sup>3</sup> and the fuel composition from 100–25% cellulose in decrements of 25% cellulose, with hemicellulose as the remaining fuel in the mixture. As Figure 4 shows, mean peak temperature increases with increasing density.<sup>1</sup> To determine the cause of this temperature dependence, we individually varied the parameters that change when density increases. We found that decreasing value of the empirical parameter for radiation across pores ( $\gamma$ ) of the condensed-phase species contributes most to the increase in peak temperatures. Figure 5 shows temperature profiles for 100% cellulose at densities of 200, 300, and 200 kg/m<sup>3</sup> but with  $\gamma$  associated with 300 kg/m<sup>3</sup>. For the fuel with a density of 200 kg/m<sup>3</sup>, when we change only the values of  $\gamma$  for the condensed-phase species to those at 300 kg/m<sup>3</sup>, the peak temperatures closely match those of the 300 kg/m<sup>3</sup> fuel, with differences of 1.9% and 1.2% for 2 cm and 3 cm profiles, respectively.

<sup>1</sup>The calculated peak temperatures differ from those shown in Figure 3 due to the different treatment of density, as we discussed in Section 2.4.

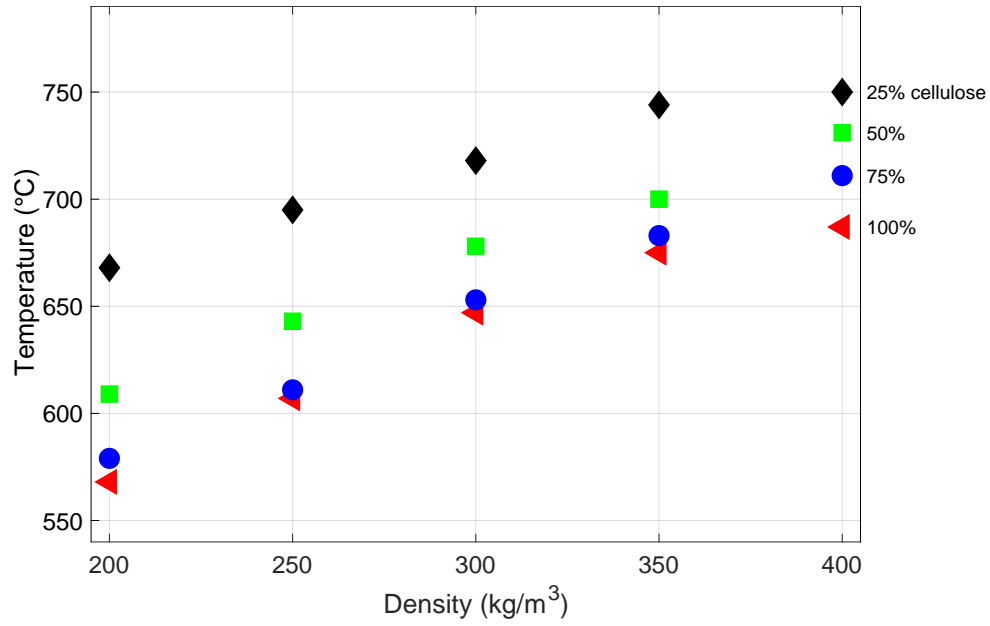


Figure 4. Effects of varying density and fuel composition on peak temperature.

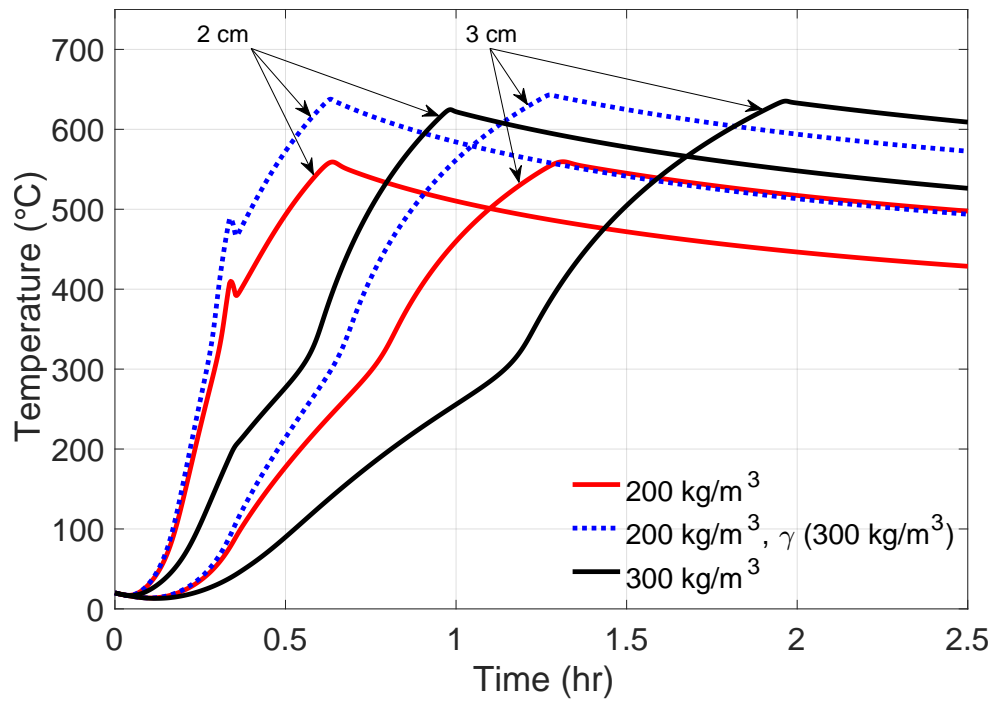
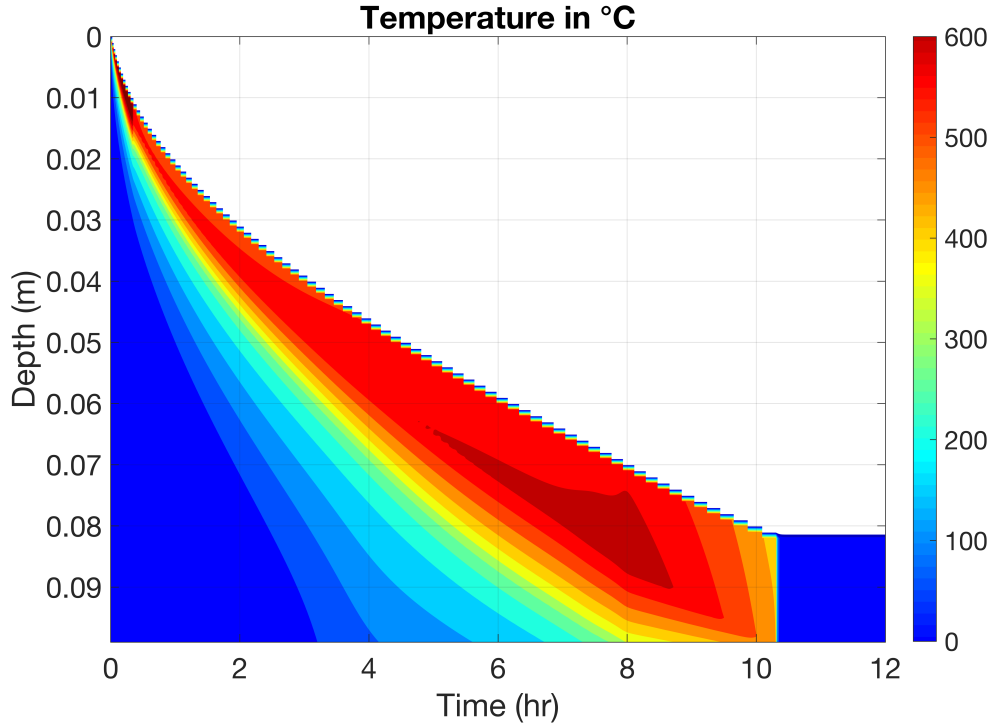


Figure 5. Temperature profiles at depths of 2 and 3 cm of 100% cellulose with densities 200 kg/m<sup>3</sup>, 300 kg/m<sup>3</sup>, and 200 kg/m<sup>3</sup> with the empirical parameter for radiation across pores ( $\gamma$ ) of 300 kg/m<sup>3</sup>.



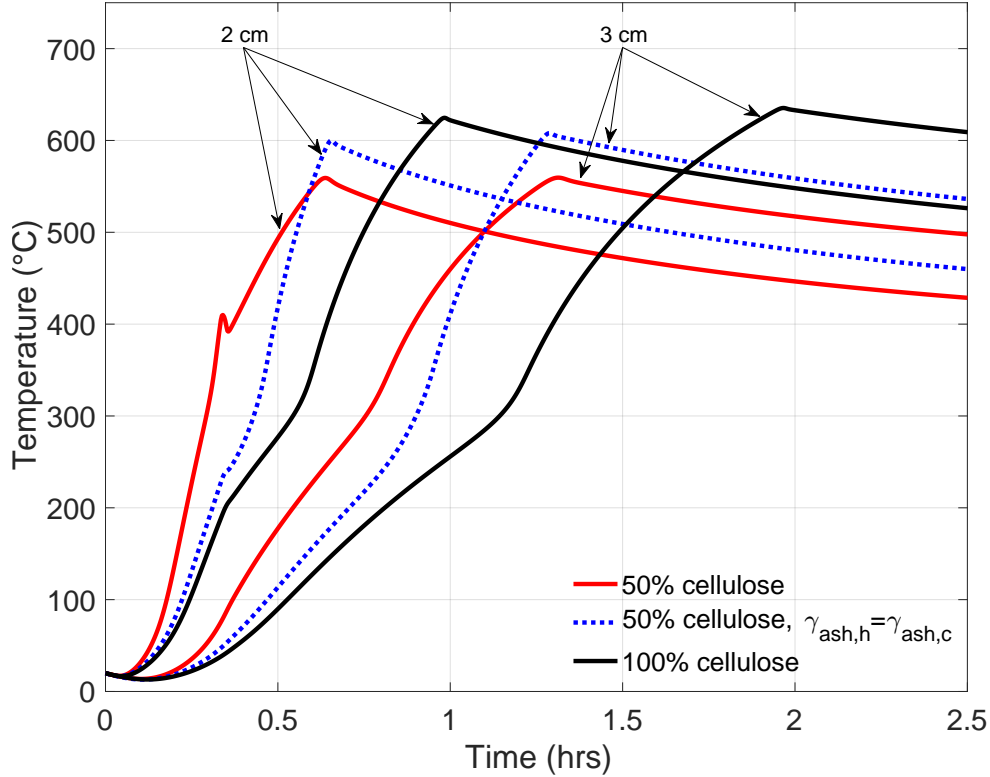
**Figure 6.** Temperature contour varying with depth and time for fuel composition of cellulose 50% and density of  $300 \text{ kg/m}^3$

Figure 4 also shows that increasing hemicellulose content in the fuel increases mean peak temperature. To explain this, Figure 6 shows temperature at varying depths and times for 50% cellulose and 50% hemicellulose at a density of  $300 \text{ kg/m}^3$ . The peak temperatures in Fig. 6 do not occur at the surface of the fuel where oxygen is most available, but instead below the surface. Ash forms at the topmost layer of the fuel, acting as an insulator. According to Eq. (20) and (22), ash formed from cellulose has a higher  $\gamma$  than ash formed from hemicellulose. This leads to greater losses due to radiation across the pores at higher cellulose content, hence peak temperatures drop with increasing cellulose content.

To test this theory, we ran a simulation with the value of  $\gamma$  of ash from hemicellulose set equal to the  $\gamma$  of ash from cellulose for a fuel mixture with 50% cellulose. In other words, in this case the ash formed from hemicellulose matches that from cellulose, in terms of radiation heat transfer across the pores. Figure 7 shows the resulting temperature profiles along with temperature profiles of 50% cellulose and 100% cellulose at density  $300 \text{ kg/m}^3$ . The peak temperature of 50% cellulose matches that of 100% cellulose when  $\gamma$  from hemicellulose matches that of ash from pure cellulose, with differences of 3.9% and 4.4% for 2 cm and 3 cm profiles, respectively.

Our findings show that the physical parameters of condensed-phase species control the observed variations in peak temperature, both as density and fuel composition change. Richter et al. [44] also discussed the larger role that physical properties play in wood charring, compared with reaction kinetics. Charring, which occurs through pyrolysis and heterogeneous oxidation, controls burning behavior and relates to temperature profile (including peak temperature). Figures 5 and 7 also show that the location of peak temperature does not shift significantly even as its value increases, In Figures 5 the shift is 0.6% and 2.3% for 2 and 3 cm profiles, and in Figures 7 the shift is 3.1%

and 2.3% for 2 and 3 cm profiles, respectively. This indicates that the change in peak temperature does not notably affect propagation speed.



**Figure 7.** Temperature profiles at depth 2 and 3 cm for fuels with density  $300 \text{ kg/m}^3$  and fuel composition of 50% cellulose, 100% cellulose, and 50% cellulose with the parameter for radiation across pores of ash coming from hemicellulose set equal to that from cellulose ( $\gamma_{ash,h} = \gamma_{ash,c}$ ).

Next, we consider the effects of density and fuel composition on mean propagation speed, shown in Figure 8. Propagation speed increases with increasing hemicellulose content and decreases with increasing density. To understand the role of fuel composition, Figure 9 shows reaction rates of fuel with hemicellulose along the depth at 4000 s. Hemicellulose pyrolyzes faster than cellulose, so that a given time its pyrolysis occurs deeper than fuels with a higher proportion of cellulose. The fuel shrinks faster, providing earlier access to oxygen ultimately leading into faster propagation speed. To examine the role of density, Figure 10 shows the reaction rates and condensed-phase species mass fractions at 4 cm below the surface for 100% cellulose at densities of  $200 \text{ kg/m}^3$  and  $300 \text{ kg/m}^3$ . The reaction rates of lower density fuel are higher and less spaced out compared to higher density fuel. This means more time is required for fuel to convert to char and ash as observed in the mass fractions of Fig. 10. This comes from the increased density of the fuel, which means more mass in a given volume converts to char and ash. As a result, the fuel shrinks, delaying access to oxygen for the char formed.

Across all fuel compositions, the propagation speed decreases by a factor of two when the density of fuel increases proportionally from  $200 \text{ kg/m}^3$  to  $400 \text{ kg/m}^3$  (i.e., doubles). Huang and Rein [14] discussed an inverse relation between oxygen concentration and density. To further examine the dependence of oxygen concentration, we increased oxygen concentration, and density simultaneously, by the same factor. The oxygen

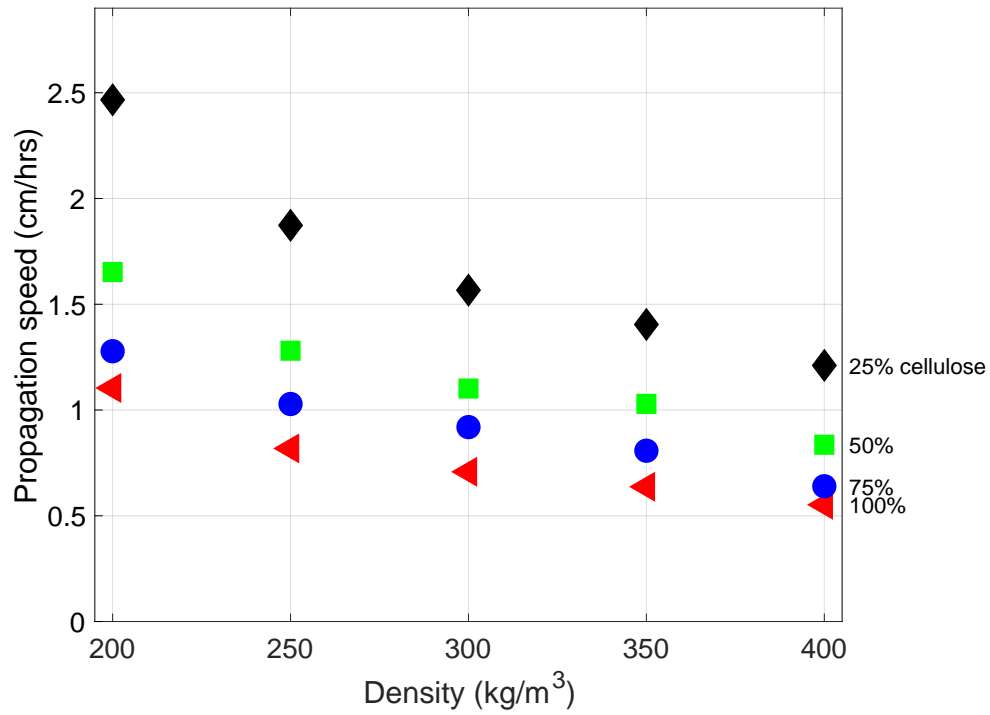


Figure 8. Effects of varying density and fuel composition on propagation speed.

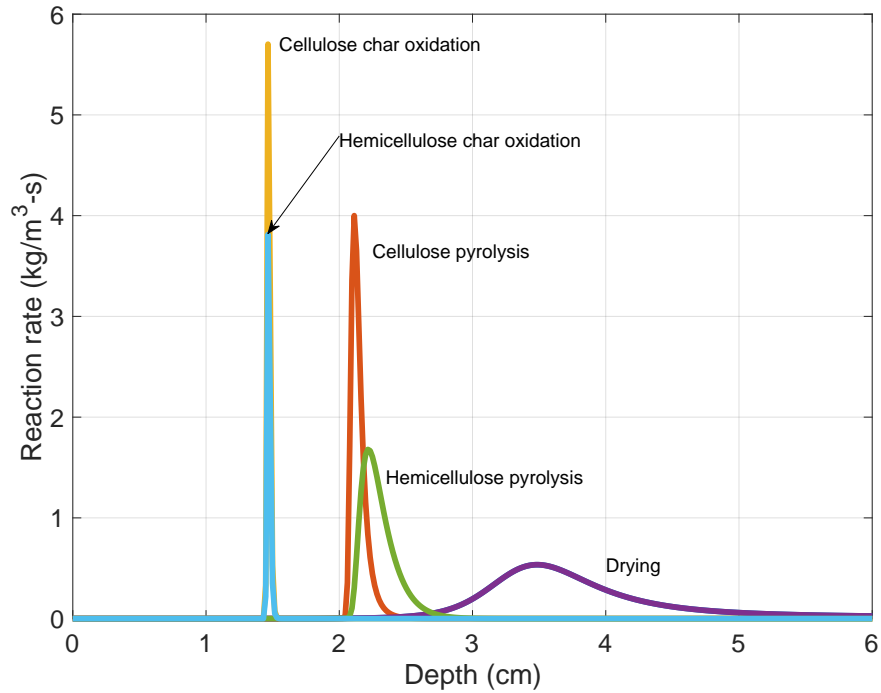
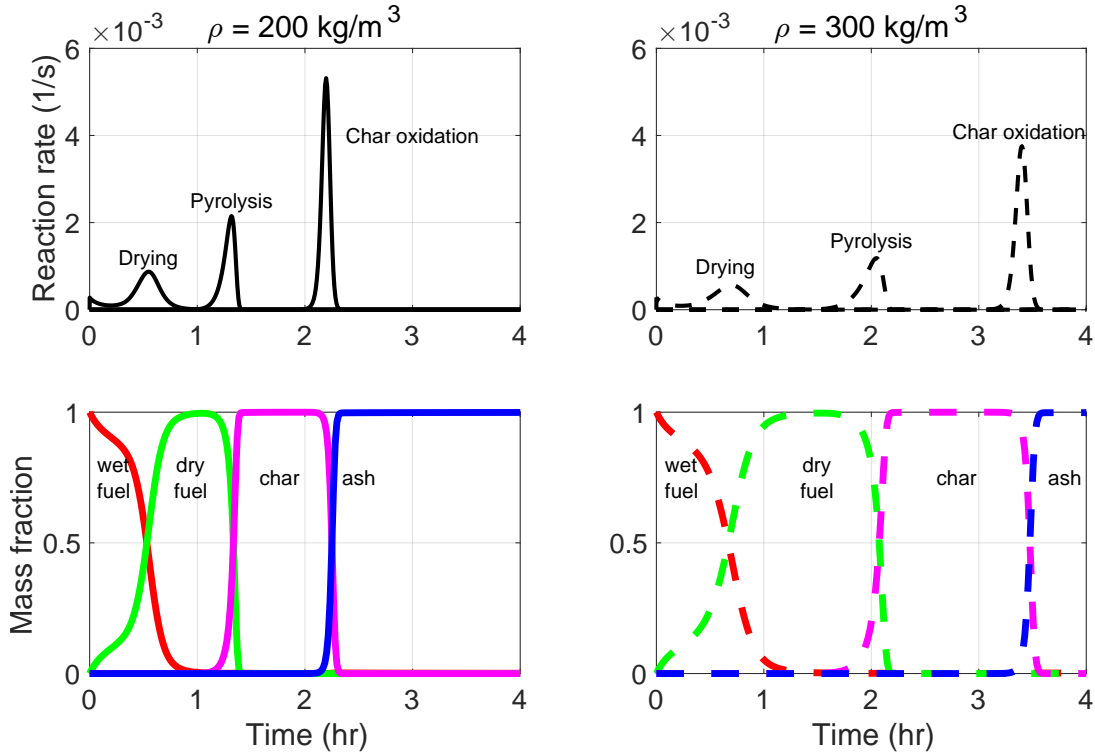


Figure 9. Reaction rates of cellulose and hemicellulose drying, pyrolysis, and oxidation for 50% cellulose and 50% hemicellulose at density 300 kg/m<sup>3</sup> along the depth at 4000 s.



**Figure 10.** Reaction rates of drying, pyrolysis, and char oxidation (top) and mass fractions of wet fuel, dry fuel, char, and ash (bottom) of 100 % cellulose with density 200 and 300 kg/m<sup>3</sup>.

supply was increased via mass fraction of (diffusing) oxygen. For example, if the density increases by a factor of 1.5, from 200 kg/m<sup>3</sup> to 300 kg/m<sup>3</sup>, then oxygen mass fraction increased to 0.348 for 300 kg/m<sup>3</sup>. This was done for all densities and fuel compositions shown in Fig. 8. Figure 11 shows that when mass fraction of oxygen ( $Y_{O_2}$ ) increases by the same factor as density ( $\rho$ ) the propagation velocities ( $S$ ) remains constant, confirming the  $S \propto Y_{O_2}/\rho$  relationship posed by Huang and Rein [14]. We performed a similar analysis of increasing oxygen supply with density for peak temperatures, shown in Figure 12; peak temperature increases with oxygen content.

To model how propagation speed and peak temperatures quantitatively scale with all the controlling variables, we performed linear regression of the data shown in Figs. 4, 8, 11, and 12. We used the Matlab function `regress()`, where the independent variables are mass fraction of cellulose ( $Y_{\text{cellulose}}$ ), density ( $\rho$ ), and oxygen concentration ( $Y_{O_2}$ ) and the dependent variables are velocity ( $S$ ) and peak temperature ( $T$ ). The resulting equations are:

$$S = 685.08 \times \frac{Y_{O_2}^{0.9892}}{\rho^{0.9464} \times Y_{\text{cellulose}}^{0.5865}} \quad \text{and} \quad (28)$$

$$T = 272.28 \times \frac{\rho^{0.2500} \times Y_{O_2}^{0.3921}}{Y_{\text{cellulose}}^{0.0835}}. \quad (29)$$

The goodness of fit ( $R^2$ ) values for both equations are approximately 0.99. In the fit for propagation speed, Eq. (28), the power of fuel density ( $\rho$ ) and mass fraction of oxygen ( $Y_{O_2}$ ) are 0.9464 and 0.9892, respectively, which are both close to 1.0—confirming the



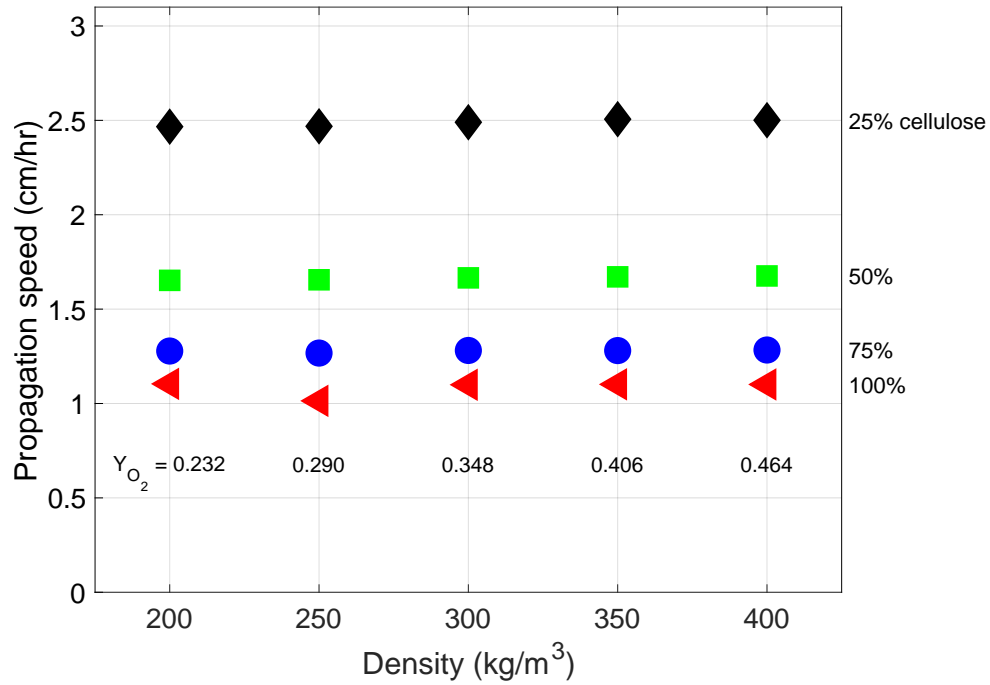


**Figure 11.** Propagation speed when oxygen availability is linearly increased with density, where the value of  $Y_{O_2}$  indicates the value of mass fraction of oxygen used for the respective density.

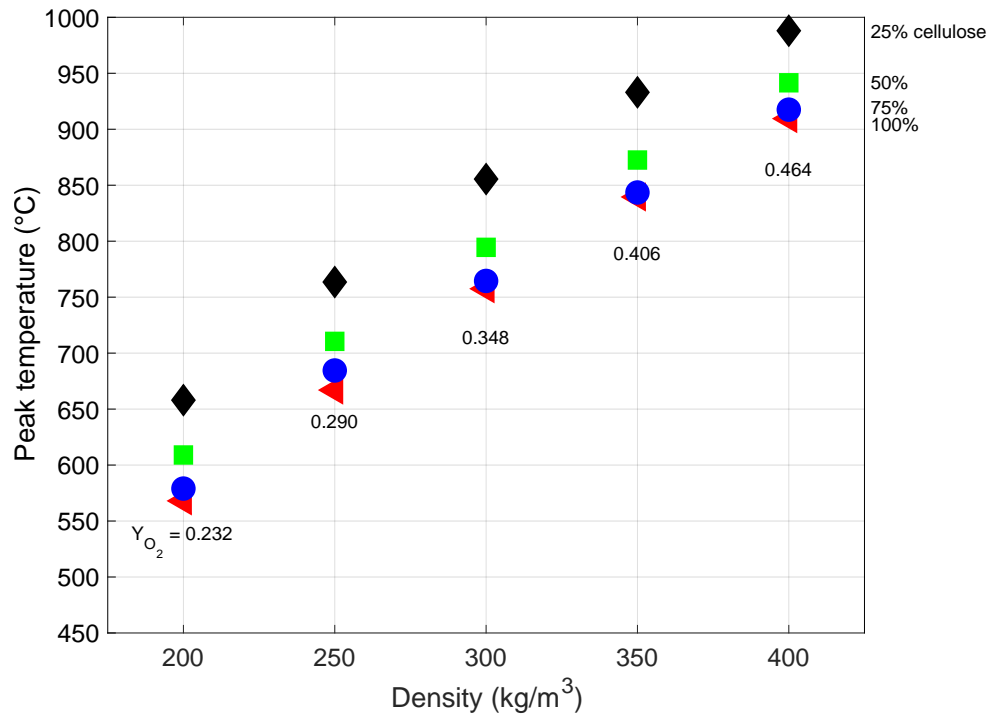


**Figure 12.** Peak temperatures when oxygen availability is linearly increased with density, where the value of  $Y_{O_2}$  indicates the value of mass fraction of oxygen used for the respective density.

$S \propto \frac{Y_{O_2}}{\rho}$  relationship discussed earlier. As demonstrated by Eq. (29), peak temperature is more sensitive to oxygen supply than to density.

### 3.3. Effect of moisture content on propagation speed

Next, we look into how moisture content affects the propagation speed and peak temperatures of smoldering, considering cases both with and without the natural expansion with water. We investigated cases without expansion because while some prior studies of peat reported expansion with addition of water [14], most woody fuels have no reported expansion.

Figure 13 shows the effect of increasing moisture content on propagation speed and peak temperature in expanding and non-expanding fuels. Moisture content is increased from 10% to 70% in increments of 20% for 100% cellulose. Peak temperature drops with increasing moisture content with and without expansion, while propagation speed shows opposite trends: increasing with expansion and decreasing without expansion.

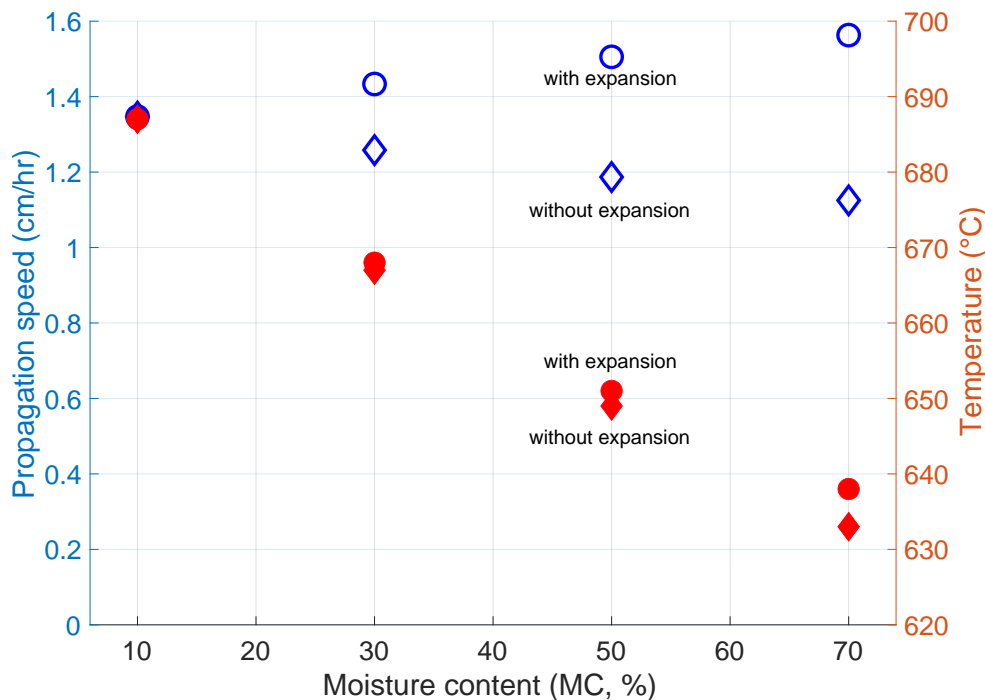


**Figure 13.** Effect of moisture content on propagation speed and peak temperature for 100% cellulose, with and without expansion, where the empty symbols indicate propagation speed and filled symbols indicate temperature.

When the fuel does not expand, i.e., all the water added to the fuel sample occupies the pores, the propagation speed decreases with increasing moisture content. In contrast, when the fuel expands, i.e., addition of water increases the total volume of the fuel, propagation speed increases with moisture content.

Without expansion, when water is added to the fuel the thermal conductivity, heat capacity, and wet fuel bulk density increase. In addition, when moisture content of the fuel increases, the drying becomes more endothermic, which increases the associated heat of reaction. To examine which parameters contribute most to reduce speed and temperature with moisture content, we analyzed the affect of each parameter individually as shown in Fig. 14. To do this, we set the value of each parameter that

changes on addition of moisture content to the value for 70% moisture content, keeping all other parameters constant. The changes in thermal conductivity and heat capacity between the two moisture contents minimally affect both propagation speed and peak temperature. Instead, the increase of (wet) bulk density is the main reason for the drop in propagation speed. In contrast, the increase in both wet bulk density and heat of reaction contribute to the drop in temperature. When increasing the wet fuel bulk density, more fuel needs to be dried by the smoldering front in a given volume, which decreases both temperature and propagation speed. When the drying reaction becomes more endothermic, more heat is required to dry the fuel, which reduces the peak temperature attained.

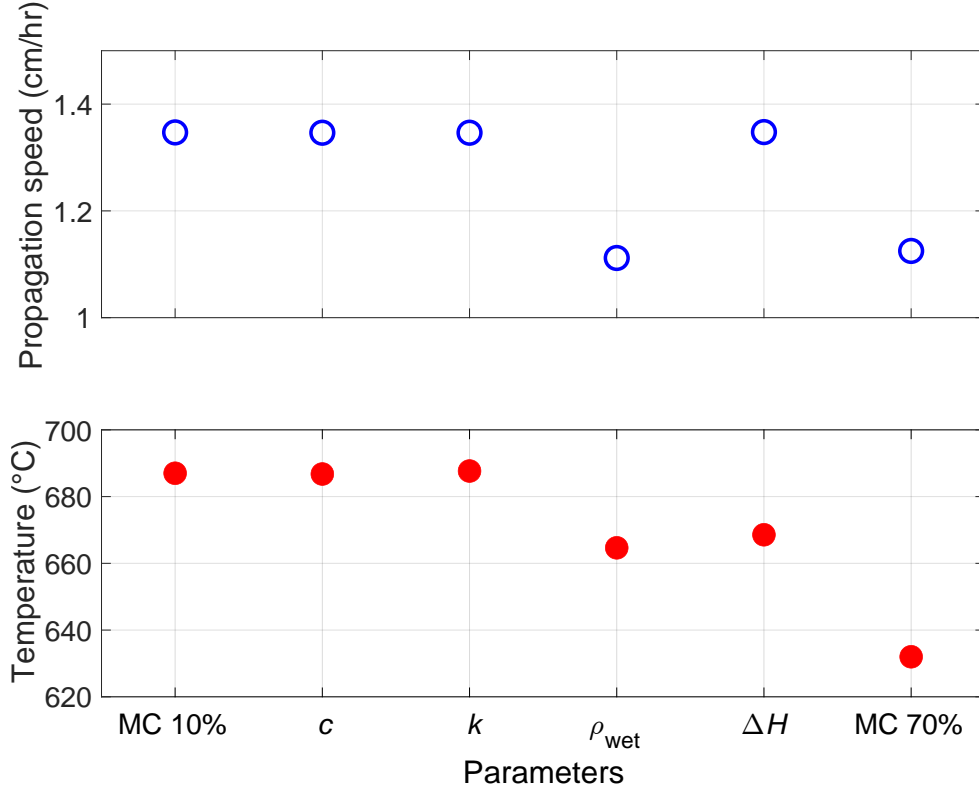


**Figure 14.** Parameter analysis for moisture content without expansion, showing impact of parameters on propagation speed (top) and peak temperature (bottom). Each parameter ( $c$ ,  $k$ ,  $\rho_{\text{wet}}$ , and  $\Delta H$ ) was changed to its value for 70% moisture content while holding all other properties to their values at 10%. These parameters increased by 55%, 48%, 58%, and 62%, respectively. The fully 10% and 70% MC cases are shown at the far left and right for comparison; note the axis scaling.

When the fuel expands with water addition, the increase in speed could be due to either the expansion of the fuel, which reduces density, or the increase in thermal conductivity. By testing the effect of each parameter, we found that changing only the thermal conductivity of the fuel negligibly impacts the propagation speed and temperature, while expansion alone increases propagation speed. When a fuel expands the overall density of the fuel decreases, and as Fig. 8 shows when the density of the fuel drops the propagation speed increases. So, in this case, propagation speed is more influenced by the overall reduction in density than the increase in the wet mass of the fuel, which increases the propagation speed. This result further confirms the relationship Huang and Rein [14] first showed for peat. The temperature reduction in

this case comes from the increasing mass of wet fuel and increasing endothermicity, similar to the case without expansion. The temperature trends are similar in both cases, since, as Eq. (29) shows, temperature is comparatively less sensitive to density and thus expansion.

### 3.4. Effect of changing composition on critical moisture content

Critical moisture content of ignition is the moisture content above which a fuel will not ignite for a given boundary condition; critical moisture content of extinction is the moisture content above which an established smoldering front does not propagate for given upstream, downstream, and boundary conditions. In this section we examine whether the critical moisture contents change with fuel composition. For this study we held density of the fuel at  $200 \text{ kg/m}^3$  and applied heat flux of  $25 \text{ kW/m}^2$  for the first 20 min to ignite the sample. We ran simulations at compositions 100%, 75%, 50%, and 25% cellulose and increased the moisture content in intervals of 10%. To measure the critical moisture content of ignition, we set a uniform moisture content throughout the fuel sample. To measure the critical moisture content of extinction, we set the top 5 cm of the domain to have 10% moisture content to ensure a self-sustained smoldering front, followed by a wet layer of 2 cm whose moisture content was systematically increased to determine the critical moisture content of extinction, with the remaining 3 cm of the sample at 10% moisture content, as shown in Figure 15.

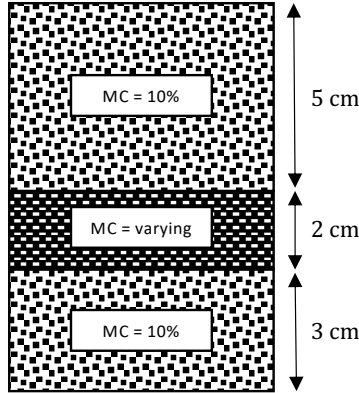


**Figure 15.** Schematic illustration of the one-dimensional computational domain with three layers of varying moisture content (MC).

**Table 3.** Critical moisture content ( $MC_c$ ) of ignition and extinction for different fuel compositions.

% Cellulose	$MC_c$ of ignition	$MC_c$ of extinction
25	40	70
50	30	60
75	30	60
100	30	60

Table 3 shows how fuel composition affects the critical moisture contents of ignition and extinction. For all compositions, critical moisture content of ignition is always lower than critical moisture content of extinction. Neither critical moisture content is

sensitive to fuel composition until the mixture contains 75% hemicellulose, when both critical moisture content of ignition and extinction increase by 10%. As previously shown in Fig. 4, adding hemicellulose to the fuel increases the mean peak temperature. At this composition, the fuel samples become hot enough to sustain smoldering combustion even at 10% higher moisture content.

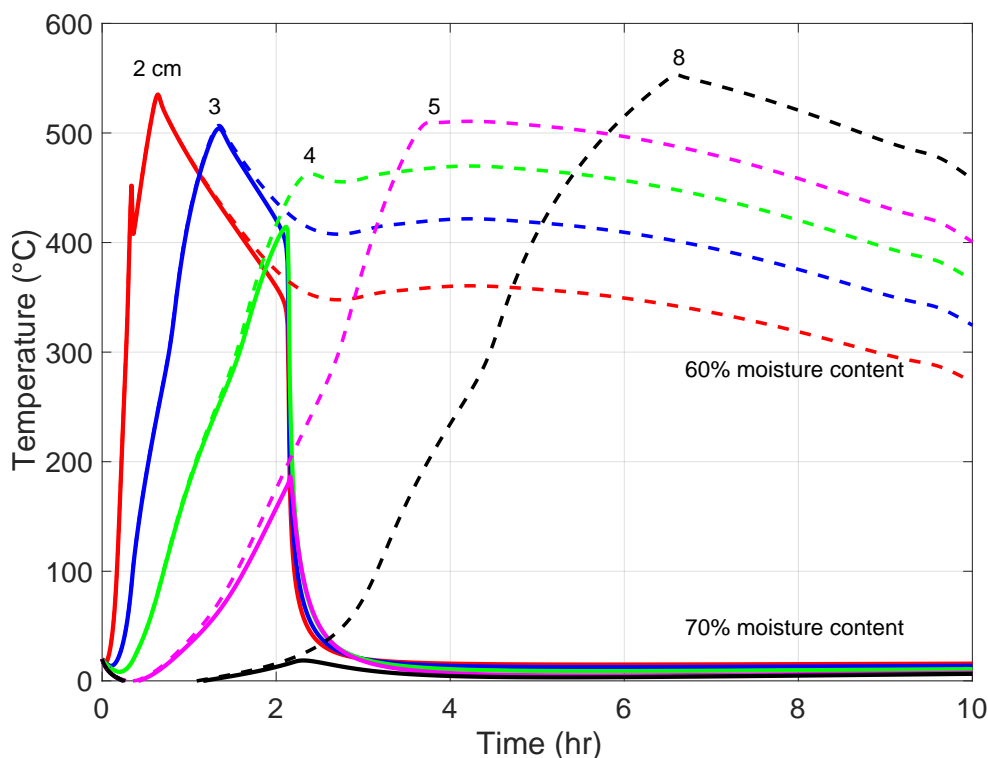


**Figure 16.** Temperature profiles of 100% cellulose with moisture content of wet layer 60% shown by dashed line and 70% shown by solid line at various depths.

Figure 16 shows the temperature profiles at different depths for fuel samples when the moisture content of the wet layer is 60% and 70%; for 60%, smoldering propagates through the wet layer, but at 70% smoldering combustion extinguishes. At 2 cm deep, the peak temperatures of the two cases match. However, as the smoldering fronts progress deeper, the difference in the moisture content downstream starts affecting the temperatures from 3 cm onward. At 4 cm deep the temperature of the 70% moisture content case drops below the point where smoldering cannot self-sustain and it extinguishes. On the other hand, the sample with 60% moisture content has a peak temperature just below 500°C at 4 cm, which is high enough to sustain smoldering. The biggest drop in the peak temperature, for the case where there was self-sustained smoldering, is approximately 1 cm above the point where the wet layer begins and not at the point of wet layer. This is because, as observed in Fig. 9, the drying process starts before char oxidation reactions using the heat liberated from char oxidation reaction along the depth of the fuel. So in this particular case, the drying of the wet layer began when char oxidation reactions were occurring approximately 1 cm above the wet layer.

## 4. Conclusions

In this work, we updated a one-dimensional computational model for smoldering combustion of cellulose and hemicellulose mixtures using the open-source software Gpyro. The model successfully predicts results from experiments at four fuel densities and compositions. We used the model to examine the impact of changing fuel composition and density on smoldering propagation speed and peak temperature. We also examined the role of moisture content, and how fuel composition affects critical moisture content of ignition and extinction.

As the density of the fuel increases, the mean propagation speed drops. This is caused by the increase in the amount of fuel that needs to be converted to ash, which slows fuel shrinkage and thus access to oxygen. In contrast, propagation speed increases with hemicellulose content in the fuel, due to the faster pyrolysis of hemicellulose compared with cellulose. Mean peak temperature also increases with additional hemicellulose content, caused by the formation of ash with lower radiation loss across pores. Mean peak temperature increases with increasing density, due to decreasing radiation losses across the pores of the fuel.

When moisture content is added and the fuel is allowed to expand, the propagation speed increases due to the reduction in density. If the fuel does not expand with the addition of water (i.e., moisture simply fills the pores), propagation speed drops primarily due to the increase in wet bulk density. Therefore, accurately modeling smoldering in a given fuel requires characterizing whether moisture content causes expansion. In both cases, additional moisture content reduces the mean peak temperature slightly. Fuel composition increases the critical moisture content of ignition and extinction only when hemicellulose becomes the major constituent, due to larger heat release.

Future studies should focus on generalizing the model to consider lignin, the third important component of biomass and woody fuels. In addition to validating a general fuel model with global outputs such as propagation speed and peak temperature, model outputs should be compared with experimental measurements of temperature profiles and mass to further-constrain the model. In addition, the impact of material and kinetic parameter uncertainty on quantities of interest should be studied. Based on the range of thermophysical parameter values (i.e.,  $\rho_{s,i}$ ,  $k_{s,i}$ ,  $c_i$ ) found in the literature [10, 14, 45–49], initial estimations suggest an uncertainty of 5–8% in propagation speed and 3% in peak temperature, which warrants a more-complete uncertainty analysis.

## Acknowledgements

We also thank David Blunck, Benjamin Smucker, and Daniel Cowan at Oregon State University for providing their experimental temperature measurements data for validation.

## Funding

This research was funded by the Strategic Environmental Research and Development Program (SERDP) award RC-2651 under contract number W912HQ-16-C-0045.

The views, opinions, and/or findings contained in this report are those of the authors and should not be construed as an official Department of Defense position of decision unless so designated by other official documentation.

## Supplementary material

The supplementary material for this article contains the complete kinetic parameters used in the model, along with additional details about the experiments used to validate the model. In addition, all of the Gpyro input files, plotting scripts, and figures are available openly under the CC-BY license [50]. Gpyro itself is available openly [24].

## References

- [1] Y. Liu, J. Stanturf, and S. Goodrick, *Trends in global wildfire potential in a changing climate*, *Forest Ecology and Management* 259 (2010), pp. 685–697, <https://doi.org/10.1016/j.foreco.2009.09.002>.
- [2] A.C. Watts and L.N. Kobziar, *Smouldering combustion and ground fires: Ecological effects and multi-scale significance*, *Fire Ecology* 9 (2013), pp. 124–132, <https://doi.org/10.4996/fireecology.0901124>.
- [3] G. Rein, *Smouldering Combustion Phenomena in Science and Technology*, *International Review of Chemical Engineering* 1 (2009), pp. 3–18, Available at <http://www.era.lib.ed.ac.uk/handle/1842/1152>.
- [4] R. Hartford and W. Frandsen, *When it's hot, it's hot... or maybe it's not! (surface flaming may not portend extensive soil heating)*, *International Journal of Wildland Fire* 2 (1992), pp. 139–144, <https://doi.org/10.1071/WF9920139>.
- [5] G. Rein, *Smouldering Fires and Natural Fuels*, in *Fire Phenomena and the Earth System*, chap. 2, Wiley-Blackwell (2013), pp. 15–33, <https://doi.org/10.1002/9781118529539.ch2>.
- [6] E. Ranzi, A. Cuoci, T. Faravelli, A. Frassoldati, G. Migliavacca, S. Pierucci, and S. Sommariva, *Chemical Kinetics of Biomass Pyrolysis*, *Energy & Fuels* 22 (2008), pp. 4292–4300, <https://doi.org/10.1021/ef800551t>.
- [7] E. Ranzi, M. Corbetta, F. Manenti, and S. Pierucci, *Kinetic modeling of the thermal degradation and combustion of biomass*, *Chemical Engineering Science* 110 (2014), pp. 2–12, <https://doi.org/https://doi.org/10.1016/j.ces.2013.08.014>.
- [8] H. Yang, R. Yan, H. Chen, D.H. Lee, and C. Zheng, *Characteristics of hemicellulose, cellulose and lignin pyrolysis*, *Fuel* 86 (2007), pp. 1781–1788, <https://doi.org/10.1016/j.fuel.2006.12.013>.
- [9] A. Anca-Couce, N. Zobel, A. Berger, and F. Behrendt, *Smouldering of pine wood: Kinetics and reaction heats*, *Combustion and Flame* 159 (2012), pp. 1708–1719, <https://doi.org/10.1016/j.combustflame.2011.11.015>.
- [10] X. Huang and G. Rein, *Thermochemical conversion of biomass in smouldering combustion across scales: The roles of heterogeneous kinetics, oxygen and transport phenomena*, *Biore-source Technology* 207 (2016), pp. 409–421, <https://doi.org/10.1016/j.biortech.2016.01.027>.
- [11] T. Kashiwagi and H. Nambu, *Global kinetic constants for thermal oxidative degradation of a cellulosic paper*, *Combustion and Flame* 88 (1992), pp. 345–368, [https://doi.org/10.1016/0010-2180\(92\)90039-R](https://doi.org/10.1016/0010-2180(92)90039-R).
- [12] B. Cagnon, X. Py, A. Guilloit, F. Stoeckli, and G. Chambat, *Contributions of hemicellulose, cellulose and lignin to the mass and the porous properties of chars and steam activated carbons from various lignocellulosic precursors*, *Biore-source Technology* 100 (2009), pp. 292–298, <https://doi.org/10.1016/j.biortech.2008.06.009>.
- [13] G. Rein, *Smouldering Combustion*, in *SFPE Handbook of Fire Protection Engineering*, Hurley M. J. et al., ed., chap. 19, Springer, New York, NY, 2016, pp. 581–603, [https://doi.org/10.1007/978-1-4939-2565-0\\_19](https://doi.org/10.1007/978-1-4939-2565-0_19).
- [14] X. Huang and G. Rein, *Downward spread of smouldering peat fire: the role of moisture, density and oxygen supply*, *International Journal of Wildland Fire* 26 (2017), pp. 907–918,

- <https://doi.org/10.1071/WF16198>.
- [15] B.D. Smucker, T.C. Mulky, D.A. Cowan, K.E. Niemeyer, and D.L. Blunck, *Effects of fuel content and density on the smoldering characteristics of cellulose and hemicellulose*, Proceedings of the Combustion Institute 37 (2019), pp. 4107–4116, <https://doi.org/10.1016/j.proci.2018.07.047>.
- [16] B.D. Smucker, T.C. Mulky, D.A. Cowan, K.E. Niemeyer, and D.L. Blunck, *Corrigendum to “effects of fuel content and density on the smoldering characteristics of cellulose and hemicellulose” [proc. combust. inst. 37 (2019) 4107-4116]*, Proceedings of the Combustion Institute 38 (2021), pp. 6781–6783, <https://doi.org/10.1016/j.proci.2020.11.004>.
- [17] E.C. Garlough and C.R. Keyes, *Influences of moisture content, mineral content and bulk density on smouldering combustion of ponderosa pine duff mounds*, International Journal of Wildland Fire 20 (2011), pp. 589–596, <https://doi.org/10.1071/WF10048>.
- [18] W.H. Frandsen, *The influence of moisture and mineral soil on the combustion limits of smoldering forest duff*, Canadian Journal of Forest Research 17 (1987), pp. 1540–1544, <https://doi.org/10.1139/x87-236>.
- [19] W.H. Frandsen, *Ignition probability of organic soils*, Canadian Journal of Forest Research 27 (1997), pp. 1471–1477, <https://doi.org/10.1139/x97-106>.
- [20] X. Huang and G. Rein, *Computational study of critical moisture and depth of burn in peat fires*, International Journal of Wildland Fire 24 (2015), pp. 798–808, <https://doi.org/10.1071/WF14178>.
- [21] X. Huang, G. Rein, and H. Chen, *Computational smoldering combustion: Predicting the roles of moisture and inert contents in peat wildfires*, Proceedings of the Combustion Institute 35 (2015), pp. 2673–2681, <https://doi.org/10.1016/j.proci.2014.05.048>.
- [22] T.C. Mulky and K.E. Niemeyer, *Computational study of the effects of density, fuel content, and moisture content on smoldering propagation of cellulose and hemicellulose mixtures*, Proceedings of the Combustion Institute 37 (2019), pp. 4091–4098, <https://doi.org/10.1016/j.proci.2018.06.164>.
- [23] B.D. Smucker, D.A. Cowan, and D.L. Blunck, Personal communication, 15 February 2018 (2018).
- [24] C. Lautenberger, *Gpyro v0.700*, <http://reaxengineering.com/trac/gpyro> (2009).
- [25] C. Lautenberger and C. Fernandez-Pello, *Generalized pyrolysis model for combustible solids*, Fire Safety Journal 44 (2009), pp. 819–839, <https://doi.org/10.1016/j.firesaf.2009.03.011>.
- [26] A. Anca-Couce, N. Zobel, A. Berger, and F. Behrendt, *Smouldering of pine wood: Kinetics and reaction heats*, Combustion and Flame 159 (2012), pp. 1708–1719, <https://doi.org/10.1016/j.combustflame.2011.11.015>.
- [27] X. Huang and G. Rein, *Smouldering combustion of peat in wildfires: Inverse modelling of the drying and the thermal and oxidative decomposition kinetics*, Combustion and Flame 161 (2014), pp. 1633–1644, <https://doi.org/10.1016/j.combustflame.2013.12.013>.
- [28] K.Y. Li, X. Huang, C. Fleischmann, G. Rein, and J. Ji, *Pyrolysis of medium-density fiberboard: Optimized search for kinetics scheme and parameters via a genetic algorithm driven by kissinger’s method*, Energy & Fuels 28 (2014), pp. 6130–6139, <https://doi.org/10.1021/ef501380c>.
- [29] C. Huggett, *Estimation of rate of heat release by means of oxygen consumption measurements*, Fire and Materials 4 (1980), pp. 61–65, <https://doi.org/10.1002/fam.810040202>.
- [30] D.A. Cowan, B.D. Smucker, and D.L. Blunck, *Sensitivity of smoldering combustion to cellulose and hemicellulose content*, in *10th US Combustion Meeting*. 2017.
- [31] X. Huang, Personal communication, 25 March 2017 (2017).
- [32] R. Moriana, Y. Zhang, P. Mischnick, J. Li, and M. Ek, *Thermal degradation behavior and kinetic analysis of spruce glucomannan and its methylated derivatives*, Carbohydrate Polymers 106 (2014), pp. 60–70, <https://doi.org/10.1016/j.carbpol.2014.01.086>.
- [33] NOSB TAP, *National Organic Standards Board Technical Advisory Panel Review on Cellulose Processing*, <https://www.ams.usda.gov/sites/default/files/media/>



- [Cellulose%20TR%202001.pdf](#) (2011). Accessed: 2017-08-29.
- [34] C-Therm Technologies, *Thermal Physical Properties Reference Library: Part II (L-R)*, [http://ctherm.com/products/tci\\_thermal\\_conductivity/helpful\\_links\\_tools/thermal\\_physical\\_properties\\_conductivity\\_effusivity\\_heat\\_capacity\\_density2/](http://ctherm.com/products/tci_thermal_conductivity/helpful_links_tools/thermal_physical_properties_conductivity_effusivity_heat_capacity_density2/) (2017). Accessed: 2017-08-29.
- [35] R. Aseeva, B. Serkov, and A. Sivenkov, *Fire behavior and fire protection in timber buildings*, Springer Series in Wood Science, Springer, Dordrecht, 2014, <https://doi.org/10.1007/978-94-007-7460-5>.
- [36] E.E. Thybring, *Explaining the heat capacity of wood constituents by molecular vibrations*, Journal of Materials Science 49 (2014), pp. 1317–1327, <https://doi.org/10.1007/s10853-013-7815-6>.
- [37] J. Eitelberger and K. Hofstetter, *Prediction of transport properties of wood below the fiber saturation point - A multiscale homogenization approach and its experimental validation. Part I: Thermal conductivity*, Composites Science and Technology 71 (2011), pp. 134–144, <https://doi.org/10.1016/j.compscitech.2010.11.007>.
- [38] R.T. Jacobsen, E.W. Lemmon, S.G. Penoncello, Z. Shan, and N.T. Wright, *Thermophysical Properties of Fluids and Materials*, in *Heat Transfer Handbook*, Vol. 1, chap. 2, John Wiley & Sons (2003), pp. 43–160.
- [39] B. Punmia and A.K. Jain, *Soil mechanics and foundations*, Laxmi Publication Pvt Limited, 2005.
- [40] F. Yu, G. Wei, X. Zhang, and K. Chen, *Two effective thermal conductivity models for porous media with hollow spherical agglomerates*, International Journal of Thermophysics 27 (2006), pp. 293–303, <https://doi.org/10.1007/s10765-006-0032-7>.
- [41] Sigma-Aldrich,  *$\alpha$ -Cellulose*, <http://www.sigmaaldrich.com/catalog/product/sigma/c8002?lang=en&region=US> (2017). Accessed: 2017-08-29.
- [42] M. Schure, P.A. Soltys, D.F.S. Natusch, and T. Mauney, *Surface area and porosity of coal fly ash*, Environmental Science & Technology 19 (1985), pp. 82–86, <https://doi.org/10.1021/es00131a009>.
- [43] Parchem, *Glucomannan*, <https://www.parchem.com/chemical-supplier-distributor/Glucomannan-007456.aspx> (2017). Accessed: 2017-08-29.
- [44] F. Richter, A. Atreya, P. Kotsovinos, and G. Rein, *The effect of chemical composition on the charring of wood across scales*, Proceedings of the Combustion Institute 37 (2019), pp. 4053–4061, <https://doi.org/10.1016/j.proci.2018.06.080>.
- [45] R.S. Miller and J. Bellan, *A generalized biomass pyrolysis model based on superimposed cellulose, hemicellulose and lignin kinetics*, Combustion Science and Technology 126 (1997), pp. 97–137, <https://doi.org/10.1080/00102209708935670>.
- [46] L.Y. Mwaikambo and M.P. Ansell, Journal of Materials Science Letters 20 (2001), pp. 2095–2096, <https://doi.org/10.1023/a:1013703809964>.
- [47] C. Qi, S. Hou, J. Lu, W. Xue, and K. Sun, *Thermal characteristics of birch and its cellulose and hemicelluloses isolated by alkaline solution*, Holzforschung 74 (2020), pp. 1099–1112, <https://doi.org/10.1515/hf-2019-0285>.
- [48] F. Richter, F.X. Jervis, X. Huang, and G. Rein, *Effect of oxygen on the burning rate of wood*, Combustion and Flame 234 (2021), p. 111591, <https://doi.org/10.1016/j.combustflame.2021.111591>.
- [49] H. Yan and O. Fujita, *Experimental investigation on the smoldering limit of scraps of paper initiated by a cylindrical rod heater*, Proceedings of the Combustion Institute 37 (2019), pp. 4099–4106, <https://doi.org/10.1016/j.proci.2018.07.049>.
- [50] T.C. Mulky, W.J. Jayasuriya, and K.E. Niemeyer, *Input files, plotting scripts, and figures for “Smoldering combustion in cellulose and hemicellulose mixtures: Examining the roles of density, fuel composition, oxygen concentration, and moisture content”*, Zenodo (2019). <https://doi.org/10.5281/zenodo.3358193>.